Multifrequency Biplanar Interferometric Imaging

Article *in* IEEE Geoscience and Remote Sensing Letters · February 2010

DOI: 10.1109/LGRS.2009.2029533 · Source: IEEE Xplore

David A. Demer
Southwest Fisheries Science Center

Multifrequency Biplanar Interferometric Imaging

George R. Cutter Jr. and David A. Demer

***Abstract*—The resolution of 3-D imaging is greatly improved using a new multifrequency biplanar interferometry (MBI) technique. Using data from a multifrequency-acoustic pulse-echo system, ranges to coherent targets, estimated from propagation delays, and the phase differences between echoes received with four quadrants of a split-aperture array are converted to Cartesian distances, and transformed into Earth coordinates. The collective data set is interpolated to create a surface closely approximating the target's image. The resolution of the resulting image is improved orders of magnitude relative to those created with measures based on echo-intensity or single-frequency uniplanar interferometry. The effectiveness of MBI is demonstrated using data from a multifrequency (18 to 200 kHz) split-aperture echosounder system to produce composite high-resolution (submeter precision) images of the seabed sensed at long ranges (tens to hundreds of meters). MBI can be broadly applied to data from split-aperture remote-sensing systems which use acoustic or electromagnetic waves.**

***Index Terms*—Acoustic imaging, echosounder, interferometry, multiple frequency.**

I. INTRODUCTION

CONTEMPORARY acoustic imaging systems are typically based on beamforming or interferometry, or a combination of these differing technologies [1]–[3]. In both cases, one estimate of range to a target is estimated per beam (beamforming) or per sample in one plane (interferometry) from the two-way propagation delay between the pulse transmission and reception. The methods differ in the way that they measure target bearing angles. To remotely image the seabed, for example, multibeam echosounders electronically form, or beamform, a swath of narrow, typically $\leq 2^\circ$, transmit and receive beams [4]. The third dimension is sampled by moving the sensor between transmissions. Generally, electronically formed beams have decreased resolution in the plane of the swath with increased target range and decreased grazing angle (these limitations can be reduced by beam focusing in range and bearing, and using nonplanar arrays, respectively). In contrast, interferometric sidescan systems [5] sample the seabed echo with multiple receivers stacked in one plane, measure one or more phase differences, and use this information to infer the angle of arrival

$$\alpha = \sin^{-1}\left(\frac{\Delta\phi}{kd}\right) \qquad (1)$$

Manuscript received May 13, 2009; revised July 2, 2009. First published October 16, 2009; current version published January 13, 2010.

The authors are with the National Oceanic and Atmospheric Administration, National Marine Fisheries Service, Southwest Fisheries Science Center, La Jolla, CA 92037 USA (e-mail: George.Cutter@noaa.gov; David.Demer@noaa.gov).

Digital Object Identifier 10.1109/LGRS.2009.2029533

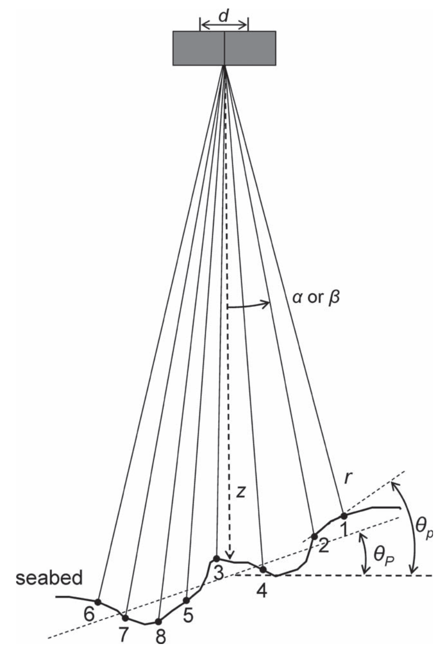

Fig. 1. For each sample p measured within the coherent seabed echo, the angles of arrival α and β in two orthogonal planes (here, measurements are illustrated in only one plane for simplicity), are estimated from the electrical phase differences detected by subarrays of the transducer that are separated by distance d; and the range r is estimated from the two-way propagation delay. The samples are sequenced with increasing range (e.g., indexed 1–8). These data are converted to horizontal x and y and vertical z Cartesian distances and transformed to Earth coordinates for fine-scale (subbeam) imaging. Fine-scale seabed slope θ_p can be estimated between multiple $x{-}y{-}z$ positions. In addition, all P of the positions within the insonified area for one transmission can be used to estimate the average slope of the seabed within the beam θ_P.

where $\Delta\phi$ is the electrical phase difference, k is the acoustic wavenumber, and d is the effective separation between two subarrays (Fig. 1). Interferometric systems have reduced measurement accuracy in cases of echoes coincidentally arriving from multiple sources, or multipath reverberation [6]. This limitation is mitigated with multiple arrival angles measured with a planar array of multiple receivers [7]. In addition, coincident echoes can be rejected, reducing measurement uncertainty, using colocated multifrequency split-aperture transducers and interferometry [8].

II. MBI METHOD AND RESULTS

We present a novel combination of these technologies—multifrequency biplanar interferometric (MBI) imaging. The MBI can be very effective and efficient if applied to data from multifrequency beamformed split-aperture multibeam echosounders, which are now commercially available [9]. In addition, MBI can probably be more broadly applied to data from split-aperture remote-sensing systems which use either acoustic or electromagnetic waves.

Compared to beamformed multibeam sonars, interferometric sidescan sonars are simpler, less expensive, and have wider swaths, but have lower angular accuracy [4]. The advantages of each technology can be exploited by applying interferometry within the narrow electronically formed beams. For example, multibeam data processing now commonly uses amplitude detections of range for near-vertical beams, when the period during which the pulse intersects the seabed is small, and phase detections of range for smaller grazing angles, when the phase differences approximate a linear function of time, with zero phase differential indicating the echo from the beam-steering direction [10]–[12]. Note, however, that acoustic interferometry has only been applied in one plane, making the phase differences appear random and noisy during times away from the zero phase differential [13]. This is due to the effects of noise [8], water-column scatterers [14], coincident echoes [6], [8], [15], and notably because the measured phases represent 3-D bearing angles projected onto one plane.

Demer *et al.* [16] introduced MBI to estimate seabed depth and slope, and indices of seabed hardness and roughness, within each beam. The method was demonstrated using split-aperture single-beam echosounders. The variance-to-mean ratio (VMR) of multifrequency echo amplitudes was used to apportion the seabed echo to coherent and incoherent components [16]. Interferometry was used on the coherent signals to measure the target bearing angles in two planes. In addition, a plane was fit to the target locations estimated from these angles to more robustly estimate $\Delta\phi = 0$, giving the vertical range to the seabed and its slope within the acoustic beam.

These estimates of range allow quantification of the volume near the seabed where its echo can eclipse those from nearby fish, the so-called acoustic dead zone, using a single multifrequency transmission [16]. The within-beam estimates of slope (Fig. 2) and the corresponding measurements of surface scattering spectra from each transmission can also be used to invert a physics-based scattering model for fine-scale estimates of hardness and roughness of the seabed [16]. Despite these advances in estimating range and within-beam slope, still, only single estimates of each parameter were derived for each transmission for each beam.

Here, we advance MBI to allow numerous estimates per transmission, which dramatically improves the resolution achievable with high-frequency remote acoustic imaging. Each of the samples within the echoes at each frequency provides independent estimates of echo range and two orthogonal bearings, which collectively allow imaging with unprecedented sub-beam precision. With this advanced implementation of MBI, the one range estimate per beam and the uniplanar sampling of the interferometric sidescan are replaced with P equal to tens to hundreds of position estimates times F frequencies which provide numerous independent yet highly correlated samples [8], [16] (Figs. 1 and 3). For each transmission, the $P \times F$ samples describe a 3-D surface within the overlapping multifrequency beams. Moreover, the numerous samples from each transmission typically overlap substantially with measures

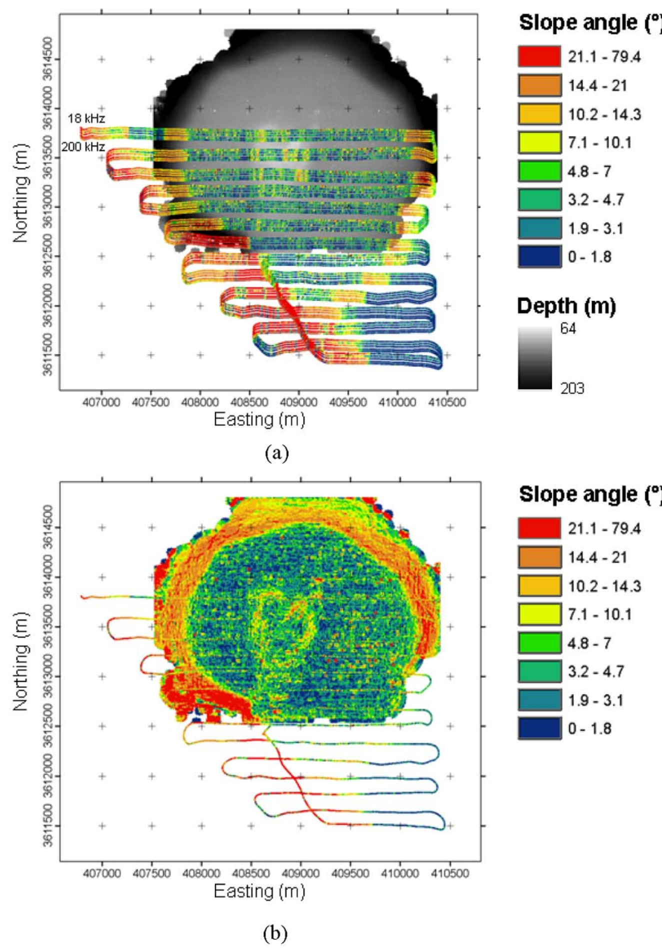

Fig. 2. (a) Within-beam seafloor slope angles estimated from MBI solutions of echosounder data (Simrad EK60) for each of the five frequencies (measurements at 18, 38, 70, 120, and 200 kHz are offset vertically) overlaid on an image of seabed bathymetry derived from multibeam echosounder data (Simrad SM20, 200 kHz) using amplitude detections. Note the high correlation between the independent measures, with some frequency dependence of the within-beam slopes. (b) Mean values of the five-frequency within-beam seafloor slopes (MBI solution) overlaid on an image of seafloor slope derived from gradients in the bathymetric surface (10 × 10 m grid cells). Note the apparent accuracy of the MBI solutions, even for near-zero slopes.

from preceding and successive transmissions and allow further improvement to the image precision.

We demonstrate the advanced MBI method using data collected from five split-aperture single-beam echosounders (Simrad EK60) to image the seabed at the 43-Fathom Bank, located approximately 40 nmi west of San Diego, CA. The 18-, 38-, 70-, 120-, and 200-kHz transducers (Simrad ES18-11, ES38B, ES70-7C, ES120-7C, and ES200-7C, respectively) were spaced to maximize the overlap of insonified volumes and minimize the vertical offsets. The transducer full beamwidths are 11° (18 kHz) and 7° (all others). The survey was conducted at a cruising speed of nominally 7 kn, and the track lines were spaced 370 m apart. At each frequency, synchronized pulses of length $\tau = 512$ μs were transmitted at 1-s intervals and propagated at the sound speed $c \approx 1515$ m $\cdot$ s^{-1}. Pulses $c\tau = 0.7757$ m long were received with bandwidths of 1.749, 3.275, 4.687, 5.557, and 5.972 kHz, corresponding to the frequencies listed above, and sampled every 128 μs, corresponding to

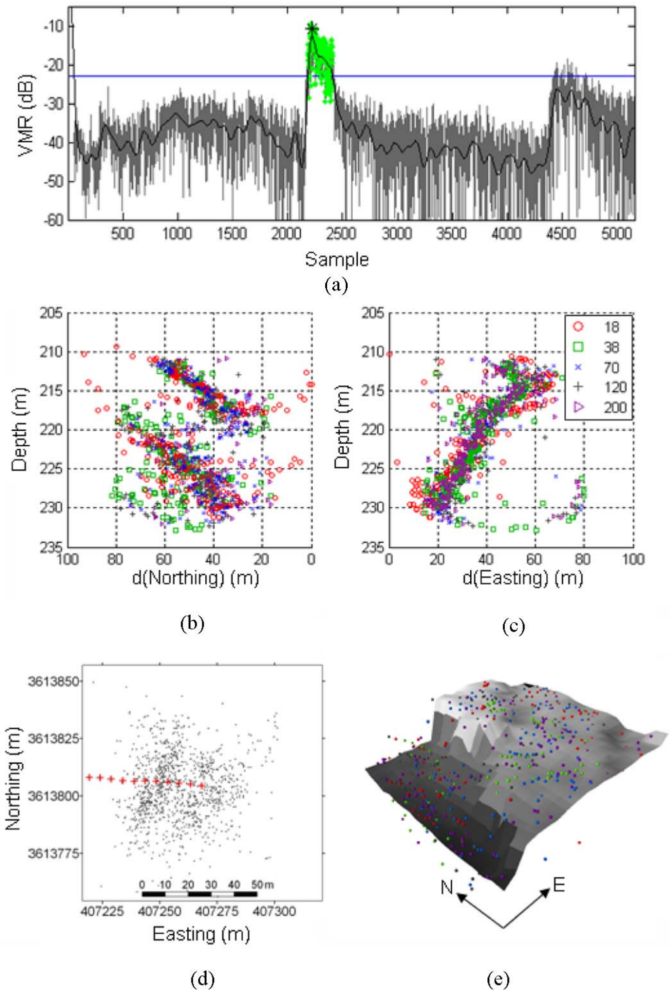

Fig. 3. (a) Coherent portion of the seabed echo (green circles) is identified by a low-pass filtered (black line) VMR of the multiple-frequency echo amplitudes at each sample exceeding an empirical threshold (e.g., -23 dB [16]; blue line). The corresponding values of α and $\beta \leq 2.5^\circ$ and r are converted to Cartesian distances and transformed to Earth coordinates. The depth profile of a ledge is shown in the (b) north-south and (c) east-west planes, with 689 measurements (compared to normally five) color coded by sampling frequency: (red) 18, (green) 38, (blue) 70, (gray) 120, and (purple) 200 kHz. (d) Plan view of image samples from a single transmission at five frequencies, and the locations of the transducers for this transmission and the preceding ten transmissions (red plus). These samples have a median resolution of ~0.6 m (compared to a standard resolution of ~26.4 m) at an observational range of 216 m. (e) High-resolution surface obtained by gridding the MBI data from a single transmission in 2×2 m cells.

four samples per pulse, providing range samples every 0.097 m. Echo amplitude (e) versus range (r), and split-aperture phase angles (α and β) corresponding to ranges up to 500 m beneath the transducers were recorded continuously for each frequency. These data were indexed by time and geographic position using data from a global positioning system receiver.

Within each beam, the number of samples from the coherent seabed echo is controlled by the acoustic frequency, pulse duration, sample rate, incidence angle, and the seabed range and morphology. The α and β, describing angles of arrival within two orthogonal planes intersecting along the beam axis, are each derived from electrical phase differences measured between transducer halves, and a conversion factor denoted angle sensitivity that is equal to the product kd in (1) (see [8] for details). Angle sensitivity is sensor specific due to its dependence on the acoustic frequency and transducer characteristics. The angular measurement precision is 0.10° for the 18-kHz system and 0.06° for the other frequencies. Each sample of α and β represents the bearing to the facet with the dominant scattering amplitude (a function of the acoustic impedance contrast and incidence angle) at that sample range. Coincident echoes will therefore cause errors in the detected amplitudes and phases [8], [15].

Noise in the echo amplitude data at 18 and 38 kHz was generally negligible. Background noise in the 70-, 120-, and 200-kHz data was removed by incoherent subtraction. Next, the VMR values from the noise-suppressed five-frequency echo amplitude data were calculated as

$$\mathrm{VMR} = 10\log\left(\frac{\frac{1}{F-1}\sum_{f=1}^{F}(e_{p,f}-\overline{e_p})^2}{\overline{e_p}}\right), \qquad \overline{e_p} = \frac{\sum_{f=1}^{F} e_{p,f}}{F} \tag{2}$$

where p indexes the samples and f indexes the frequencies for each transmission [16]. A low-pass filtered VMR ≥ -23 dB (estimated empirically as in [16]) were used to identify minimum and maximum ranges of the coherent seabed echoes (Fig. 3). P sets of samples within the coherent seabed echoes ($\alpha_{p,f}$, $\beta_{p,f}$, and $r_{p,f}$) were converted to P sets of Cartesian distances ($x_{p,f}$, $y_{p,f}$, and $z_{p,f}$) following [17]:

$$\begin{bmatrix} x_{p,f} \\ y_{p,f} \\ z_{p,f} \end{bmatrix} = \frac{r_{p,f}}{\sqrt{1-\sin^2\alpha_{p,f}\sin^2\beta_{p,f}}}\begin{bmatrix} \sin\alpha_{p,f}\cos\beta_{p,f} \\ \cos\alpha_{p,f}\sin\beta_{p,f} \\ \cos\alpha_{p,f}\cos\beta_{p,f} \end{bmatrix} \tag{3}$$

and transformed into Earth coordinates. These independent multifrequency estimates of 3-D target positions are highly correlated so their combination enhances the resolution of image features. Noisy estimates with low correlations were rejected if their VMR did not exceed a threshold of -17 dB. The collective data set was then interpolated to create a high-resolution (submeter precision) 3-D surface of the seabed sensed at ranges of 80 to 500 m (Fig. 4). The seabed image depicts shapes of bathymetric features which are larger than a wavelength, and indicates the within-beam seabed roughness.

III. Discussion

These results can be further improved with account for sound refraction, transducer displacements [8], and transducer pitch, roll, yaw [17], and heave. In addition, the echo intensity of each multifrequency sample can be normalized for the acoustic incidence angle, estimated from the gradient between adjacent samples, and used to estimate sub-beam seabed hardness and roughness, as in [16] but with orders of magnitude higher resolution. MBI can even be applied to archived split-aperture data to extract much more information about target shapes and morphologies. When validating these interpretations, it is

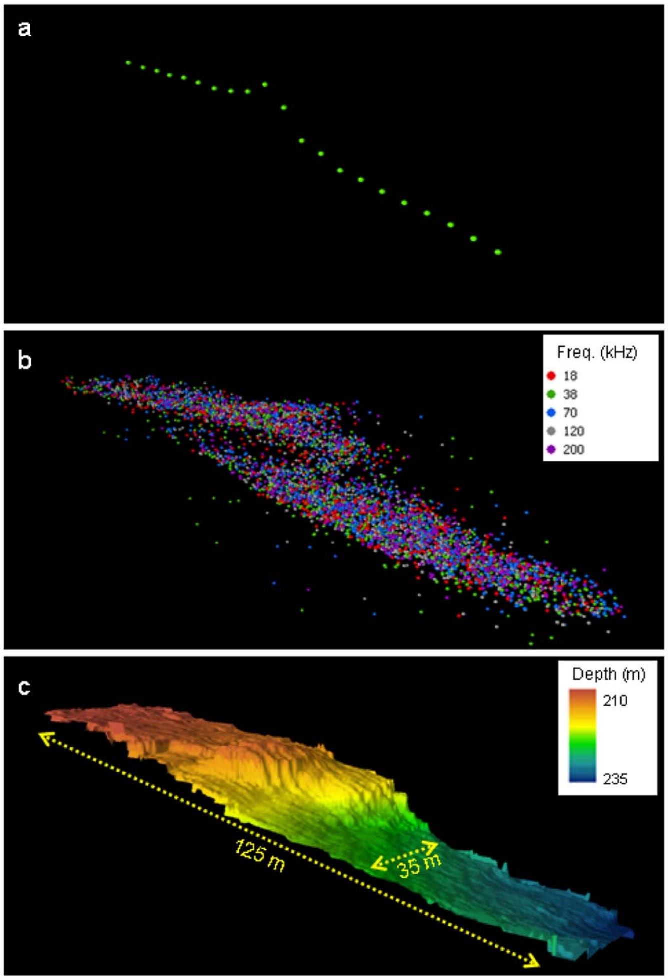

Fig. 4. MBI images of the seabed estimated using data from multifrequency split-aperture echosounders. (a) Using standard methods, each transmission from a single beam would produce a single estimate of range to the surface providing a series of point estimates as the device moved through space. (b) Using the MBI method, each transmission and beam results in tens to hundreds of range estimates (beamwidth and bandwidth dependent) and their corresponding directions that multiply with subsequent transmissions. The 5865 MBI solutions (colored by frequency) from 21 transmissions from the moving sensor (possible also by a single transmission and fan of multiple beams) produces (c) a detailed 3-D image of the seabed (0.5 × 0.5 m grid cell surface interpolated from median depth values) depicting two subbeam ledges; standard methods would have depicted this surface as a linear profile.

notable that the greatly increased resolution of MBI images, even at large ranges, allows fine-scale (ca. 1 m^2) comparisons or validations of acoustic target classifications (e.g., seabed types) made with photographs (e.g., from cameras on a remotely operated vehicle [16]) or physical samples (e.g., grab, cores, or dredges).

The empirical VMR threshold is probably dependent on the chosen set of frequencies and beamwidths and may need to be re-estimated for MBI processing of data from other systems. However, for a particular echosounder system, the echoes from various target types (e.g., seabed, fish) and even differing compositions of types (e.g., homogenous versus heterogeneous seabed or animal aggregation morphologies) may have characteristic VMR values that can be used for objective recognition and classification [16]. Consequently, there are numerous possibilities for designing sensors and processing algorithms to optimize MBI imaging of various targets.

Contrary to single-frequency multibeam systems which achieve high resolution through narrow beamwidths and short pulse durations, MBI is most efficient with wide beamwidths because they decrease the probability of near-normal incidence angles and increase the spatial sampling. The probability of near-normal incidence angles is also lowered with increased beam-steering, seabed roughness, and transducer motion. In addition, contrary to conventional processing schemes, longer pulse durations further increase the spatial sampling and the signal-to-noise ratio when using MBI. Therefore, MBI processing of data from wide-beamwidth broad-bandwidth systems with long pulses should provide even higher image resolution and precision than demonstrated here.

IV. Conclusion

The greatly increased resolution of the enhanced MBI method provides more information about target shape and morphology. This remote fine-scale imaging and classification can be achieved efficiently over large areas by applying MBI to data from broad-bandwidth split-aperture multibeam echosounders such as the Simrad ME70 [9], enabling seafloor mapping, for example, with much higher resolution and efficiency using the same vessels and sensors.

If global ocean bathymetric mapping is to be done from ocean vessels [18], then MBI offers the potential to increase the resolution of products from these expensive and time-consuming efforts. Fortunately, MBI processing can also be used to extract much more information from the large worldwide archive of multifrequency split-aperture data. MBI images have resolutions which approach those of conventional photographic and direct sampling validation methods. Moreover, MBI is applicable to data from a variety of remote-sensing systems using either acoustic (e.g., multibeam echosounders, acoustic cameras, and medical ultrasound imaging systems) or electromagnetic waves.

References

[1] H. Medwin and C. Clay, *Fundamentals of Acoustical Oceanography*. Boston, MA: Academic, 1998.

[2] X. Lurton, *An Introduction to Underwater Acoustics: Principles and Applications*. New York: Springer-Verlag, 2002.

[3] J. E. Hughes Clarke, "Applications of multibeam water column imaging for hydrographic survey," *Hydrogr. J.*, vol. 120, no. 3, pp. 3–15, 2006.

[4] C. de Moustier, "State of the art in swath bathymetry systems," *Int. Hydrogr. Rev.*, vol. 65, no. 25, pp. 25–54, 1988.

[5] M. A. Masnadi-Shirazi, C. P. de Moustier, P. Cervenka, and S. H. Zisk, "Differential phase estimation with the SEAMARC II bathymetric sidescan sonar system," *IEEE J. Ocean. Eng.*, vol. 17, no. 3, pp. 239–251, Jul. 1992.

[6] P. H. Kraeutner and J. S. Bird, "Resolving multiple angles-of-arrival in swath bathymetric imaging," in *Proc. MTS/IEEE OCEANS*, Seattle, WA, Sep. 13–16, 1999, pp. 37–45.

[7] P. H. Kraeutner, J. S. Bird, B. Charbonneau, D. Bishop, and F. Hegg, "Multi-angle swath bathymetry sidescan quantitative performance analysis," in *Proc. MTS/IEEE OCEANS*, Biloxi, MS, Oct. 29–31, 2002, pp. 2253–2263.

[8] D. A. Demer, M. A. Soule, and R. P. Hewitt, "A multi-frequency method for improved accuracy and precision of in situ target strength measurements," *J. Acoust. Soc. Amer.*, vol. 105, no. 4, pp. 2359–2376, 1999.

[9] V. M. Trenkel, V. Mazauric, and L. Berger, "The new fisheries multibeam echosounder ME70: Description and expected contribution to fisheries research," *ICES J. Mar. Sci.*, vol. 65, no. 4, pp. 645–655, 2008.

[10] C. P. de Moustier, "Signal processing for swath bathymetry and concurrent seafloor acoustic imaging," in *Acoustic Signal Processing for Ocean Exploration*, *ASI Series*, J. M. F. Moura and I. M. G. Lourtie, Eds. Norwell, MA: Kluwer, 1993, pp. 329–354.

[11] G. Shippey, "Simple algorithms for sonar imaging and bathymetry with a linear swept-frequency (chirp) source," *Int. J. Imaging Syst. Technol.*, vol. 8, no. 4, pp. 359–376, 1997.

[12] S. Bourguignon, L. Berger, C. Scalabrin, R. Fablet, and V. Mazauric, "Methodological developments for improved bottom detection with the ME70 multibeam echosounder," *ICES J. Mar. Sci.*, vol. 66, no. 6, pp. 1015–1022, 2009.

[13] L. Yang and T. Taxt, "Multibeam sonar bottom detection using multiple subarrays," in *Proc. MTS/IEEE OCEANS*, 1997, vol. 2, pp. 932–938.

[14] D. N. MacLennan, P. J. Copland, E. Armstrong, and E. J Simmonds, "Experiments on the discrimination of fish and seabed echoes," *ICES J. Mar. Sci.*, vol. 61, no. 2, pp. 201–210, 2004.

[15] K. G. Foote, "Coincidence echo statistics," *J. Acoust. Soc. Amer.*, vol. 99, no. 1, pp. 266–271, Jan. 1996.

[16] D. A. Demer, G. R. Cutter, J. S. Renfree, and J. L. Butler, "A statistical-spectral method for echo classification," *ICES J. Mar. Sci.*, vol. 66, no. 6, pp. 1081–1090, 2009.

[17] S. G. Conti, D. A. Demer, M. A. Soule, and J. H. E. Conti, "An improved multiple-frequency method for measuring *in situ* target strengths," *ICES J. Mar. Sci.*, vol. 62, no. 8, pp. 1636–1646, 2005.

[18] M. J. Carron, P. R. Vogt, and W.-Y. Jung, "A proposed international long-term project to systematically map the world's ocean floors from beach to trench: GOMaP (Global Ocean Mapping Program)," *Int. Hydrogr. Rev.*, vol. 2, no. 3, p. 49, 2001.